

APPROACHES TO GEOMETRIC DATA ANALYSIS ON BIG AREA ADDITIVELY MANUFACTURED (BAAM) PARTS

G. D. Dreifus*, *, Y. Jin†, N. Ally*, B. K. Post*

*Manufacturing Demonstration Facility, Oak Ridge National Laboratory
NTRC II, 2370 Cherahala Blvd
Knoxville, TN, 37932

† Mork Family Department of Chemical Engineering and Materials Science, University of
Southern California, Los Angeles, CA, 90007

Abstract

The promise of additive manufacturing is that a user can design and print complex geometries that are very difficult, if not impossible, to machine. The capabilities of 3D printing are restricted by a number of factors, including properties of the build material, time constraints, and geometric design restrictions. In this paper, a thorough accounting and study of the geometric restrictions that exist in the current iteration of additive manufacturing (AM) fused deposition modeling (FDM) technologies on a large scale are discussed. Offline and online methodologies for collecting data sets for qualitative analysis of large scale AM, in particular Oak Ridge National Laboratory's (ORNL) big area additive manufacturing (BAAM) system, are summarized. In doing so, a survey of tools for designers and software developers is provided. In particular, strategies in which geometric data can be used as training sets for smarter AM technologies in the future are explained.

Introduction

Additive manufacturing (AM) is a \$4.1 billion industry that is currently growing at a rate of 35.2% [1]. AM is a means of depositing material layer-by-layer to build a part from the bottom up; in fused deposition modeling (FDM), an extruder-based printer deposits a bead of material along a tool path onto a printer bed [3]. Oak Ridge National Laboratory's (ORNL) Manufacturing Demonstration Facility (MDF), along with Cincinnati Inc (CI), designed a large scale 3D printer capable of depositing material at rates almost 100 times that of typical desktop printers [7, 8]. In large scale AM, successful prints are determined by a number of varying factors. The speed of the printer gantry and the bead width of the printed material can fluctuate unexpectedly and so represent noise extent throughout the printing the process. Also, the materials and thermal properties inherent in the print create noise during the process. As a particular material cools, warping often occurs in unpredictable ways, propagating error throughout a printed part.

The geometry of a given print affects all of these parameters. A part with high curvature or sharp, sudden angles in its geometry will cause high acceleration on the printer head motion, and acceleration creates sudden changes in the flow rate of a printed material. Furthermore, while a proportional-integral-derivative (PID) controller might be used to stabilize the velocity of a printer head, a feedback mechanism to keep the acceleration stable would operate too slowly for the system to remain stable. Thus, high curvature and sharp angles create fluctuations in the bead

width during a print. Geometry can also affect a print as if is highly variable, as this will likewise cause changes in the printer head velocity.

This noise exists on the perimeter and interior of the print. On the perimeter, noise is caused by changes in velocity. In the interior, changes in velocity are similarly inevitable, but the infill tool path is influenced by the geometry of the part too. Tool path density and trajectory will have an impact on print viability and build success.

To combat these obstacles, scan data on rudimentary part geometries was collected to begin development of an open source training set that might be used to better learn tool paths and do analysis on AM build failures. The literature on deviation analysis in BAAM printing is seemingly sparse. Work has been conducted to understand deviation in stereolithography [10,11]. Deviation models have been developed that consider parametric models of FDM printing that seeks to correct for geometric part error in the CAD model [5,12]. A deviation analysis is presented here for large scale systems and potential strategies to overcome part defects in a given geometry are consequently discussed. This part serves as inspiration for potential intersections of machine learning, tool path planning, and controls.

Experiments

A series of triangles with a variety of angles on the BAAM-CI system was printed. The BAAM-CI printer was developed by ORNL in conjunction with Cincinnati Inc. and can print components as large as 20-ft. long, 8-ft. wide, and 6-ft. tall. It uses a single-screw extruder to deposit feedstock material [7]. For this experiment, 20% carbon fiber reinforced ABS was used. The pellet feedstock material is ~3.45mm in diameter and ~3.75mm in length. Triangles were printed whose CAD models had angle ratios of 90°-80°-10°, 90°-70°-20°, 90°-60°-30°, and 90°-50°-40°, as can be seen in figures 1-2 and 4-7. A 12-in. by 42-in. rectangular block with pillars and holes of various sizes in it was also printed, as can be seen in a topographical deviation analysis image in table 7. A sinusoidal wave with 6-in. amplitude appended to a 43.99-in. by 3.99-in. block was printed as well and can be seen in table 7.

Table 1: The dimensions of the triangle prints completed on the FaroArm Laser Scanner.

BAAM Prints	80-10	70-20	60-30	40-50	Sinusoidal	40-50
Base Length (in.)	2.12''	4.37''	6.93''	10.07''	43.99''	42''
Height (in.)	12''	12''	12''	12''	9.99''	12''
Hypotenuse Length (in.)	12.19''	12.77''	13.86''	15.66''	N/A	N/A

Scanning AM parts to test deviation analysis and understand part quality has been conducted [4]. To build offline training sets, a Faro Platinum Laser Arm Scanner was used to scan point clouds of each object. Mesh triangulations of a surface geometry were calculated using 3D Systems' 2015 Geomagic Software, yielding a deviation analysis between the scanned point clouds and the CAD models. The training sets can be seen in tables 1 through 7. Each table lists a range, denoted ">=Min" to "<Max," of deviation in the orthonormal direction from the surface

geometry of the CAD model and the number and percentage of points within the point cloud that exist within that given range.

Table 2: Deviation Distribution (80-10°)

>=Min	<Max	# Points	%
-0.5999	-0.4999	481	0.1133
-0.4999	-0.3999	2067	0.4867
-0.3999	-0.3000	1430	0.3367
-0.3000	-0.2000	2097	0.4938
-0.2000	-0.1000	4486	1.0563
-0.1000	0.0000	95703	22.5355
0.0000	0.1000	236298	55.6418
0.1000	0.2000	69154	16.2839
0.2000	0.3000	11397	2.6837
0.3000	0.3999	1330	0.3132
0.3999	0.4999	233	0.0549

Table 3: Deviation Distribution (70-20°)

>=Min	<Max	# Points	%
-3.0000	-2.4200	11297	2.3327
-2.4200	-1.8400	11708	2.4176
-1.8400	-1.2600	16972	3.5045
-1.2600	-0.6800	30964	6.3937
-0.6800	-0.1000	45125	9.3178
-0.1000	0.1000	19166	3.9576
0.1000	0.6800	62443	12.8938
0.6800	1.2600	59006	12.1841
1.2600	1.8400	44245	9.1361
1.8400	2.4200	36469	7.5305
2.4200	3.0000	30505	6.2990

Figure 1: Deviation analysis on a scan of a triangle with angle degrees of 90-10-80.

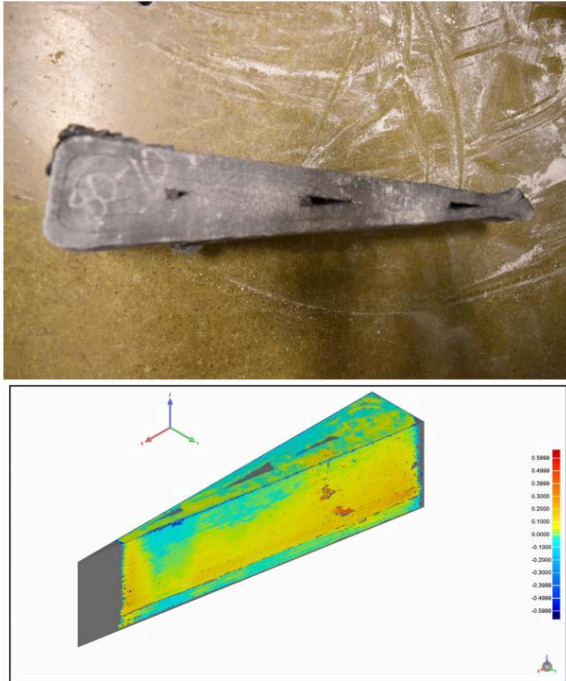
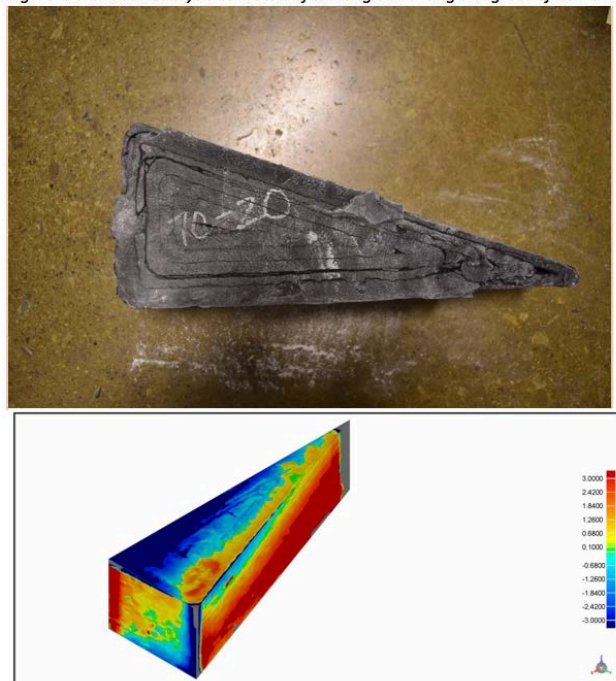


Figure 2: Deviation analysis on a scan of a triangle with angle degrees of 90-20-70.



Previously, infrared camera footage was used to analyze AM metal parts [2]. For online experiments, a FLIR Laser Scanner was attached to ORNL's BAAM system. The BAAM system was developed by ORNL and is capable of printing components 3.28-ft long, 7.87-ft wide, and 5.9-ft tall. It runs a single-screw extruder using pellet feedstock material, in this case 20% carbon fiber reinforced ABS [7]. The pellet feedstock size is ~ 0.136in. in diameter and ~0.148in. in length.

Experimentation was conducted on the ORNL BAAM machine with an infrared FLIR AX5 camera. The camera has a focal length of 19-in. so a clamp was designed to attach the FLIR camera to the side of the extruder at the requisite distance from the printer bed. The camera runs at a frequency of 30 Hz and has a resolution of 320 by 256 pixels. An online bead width measurement of a given print can now be captured, giving an accurate online measurement of printer flow rate.

The FLIR camera can capture online measurements of the width of the bead extruded from the printer head. By clamping a camera to the side of the extruder, flow rate measurements can be read throughout a given print. While FLIR cameras capture temperature alone, we used a MATLAB filter to derive the width of the bead from differences in the temperature values captured in the pixels. The color values can be captured in a matrix and filtered into a binary grey scale value.

The BAAM system's controls run off the machining language G-Code which assigns the location and velocity of the gantry that moves the extruder. We can run the MATLAB filter on a video feed of the print. Using this and the video feed from the FLIR camera allows for the calculation of a local deviation analysis of the printed material for a given part. These measurements can be made online or stored in a database to be processed for later analysis.

Figure 3: The FLIR camera image before and after the image processing of the temperature values, from which bead width can be derived.

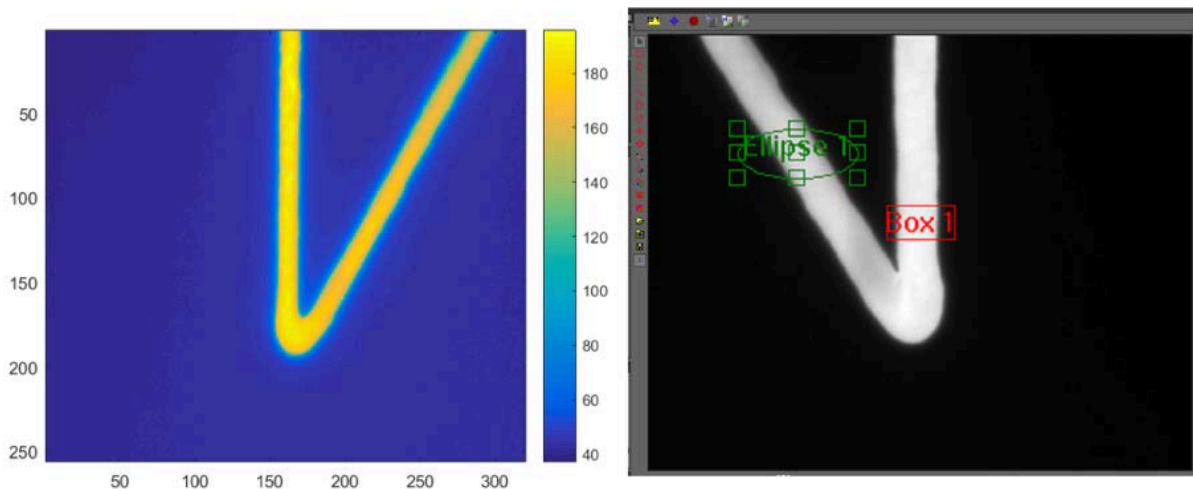


Table 4: Deviation Distribution (60-30°)

>=Min	<Max	# Points	%
-3.0000	-2.4200	11297	2.3327
-2.4200	-1.8400	11708	2.4176
-1.8400	-1.2600	16972	3.5045
-1.2600	-0.6800	30964	6.3937
-0.6800	-0.1000	45125	9.3178
-0.1000	0.1000	19166	3.9576
0.1000	0.6800	62443	12.8938
0.6800	1.2600	59006	12.1841
1.2600	1.8400	44245	9.1361
1.8400	2.4200	36469	7.5305
2.4200	3.0000	30505	6.2990

Figure 4: Deviation analysis on a scan of a triangle with angle degrees of 90-30-60.

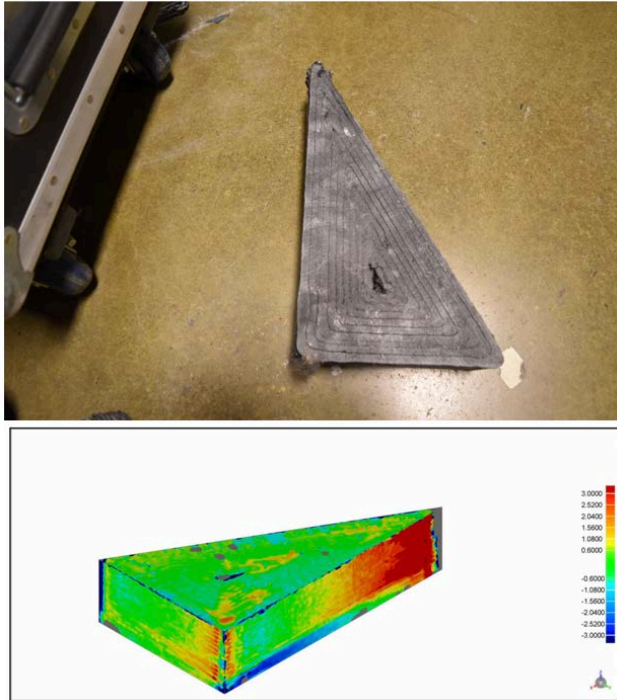


Table 5: Deviation Distribution (50-40°)

>=Min	<Max	# Points	%
-0.5996	-0.5004	1335	0.1756
-0.5004	-0.4012	997	0.1311
-0.4012	-0.3020	1480	0.1947
-0.3020	-0.2028	1591	0.2093
-0.2028	-0.1036	9055	1.1910
-0.1036	-0.0044	206902	27.2126
-0.0044	0.0044	94200	12.3896
0.0044	0.1036	289552	38.0831
0.1036	0.2028	90592	11.9150
0.2028	0.3020	53101	6.9841
0.3020	0.4012	11213	1.4748
0.4012	0.5004	293	0.0385
0.5004	0.5996	4	0.0005

Figure 5: Deviation analysis on a scan of a triangle with angle degrees of 90-40-50.

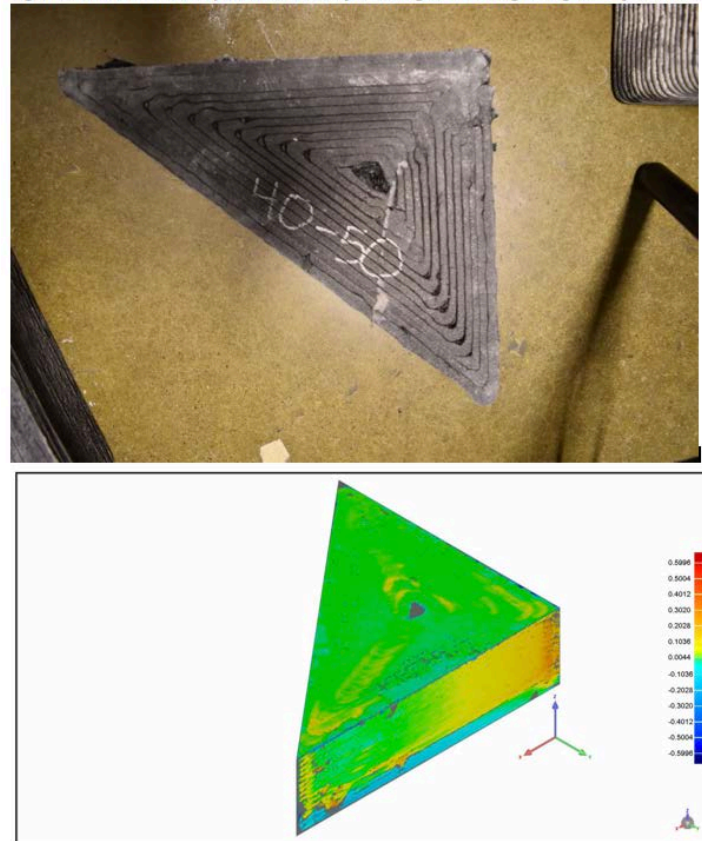


Table 6: Deviation Distribution (Sinusoidal Waves)

>=Min	<Max	# Points	%
-2.5714	-2.1429	4817	0.1410
-2.1429	-1.7143	39080	1.1440
-1.7143	-1.2857	48350	1.4154
-1.2857	-0.8571	75813	2.2193
-0.8571	-0.4286	151623	4.4385
-0.4286	0.0000	1353611	39.6245
0.0000	0.1500	1499385	43.8918
0.1500	0.3000	212857	6.2310
0.3000	0.4500	4110	0.1203
0.4500	0.6000	4385	0.1284
0.6000	0.7500	3816	0.1117
0.7500	0.9000	3223	0.0943
0.9000	1.0500	2724	0.0797

Figure 6: Deviation analysis on a scan of a sinusoidal sample print.

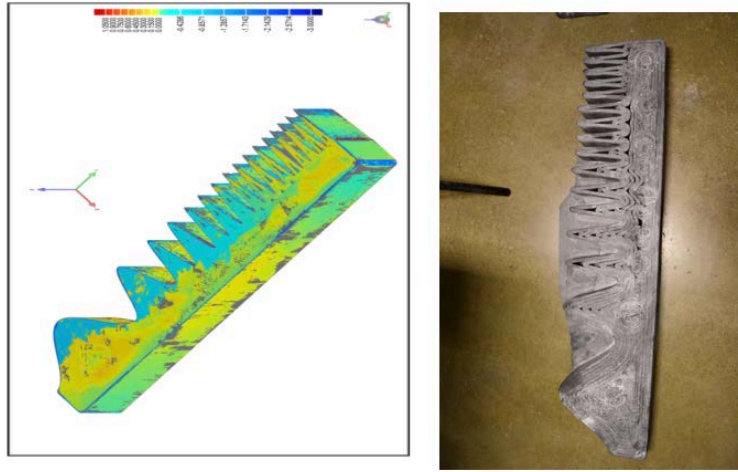
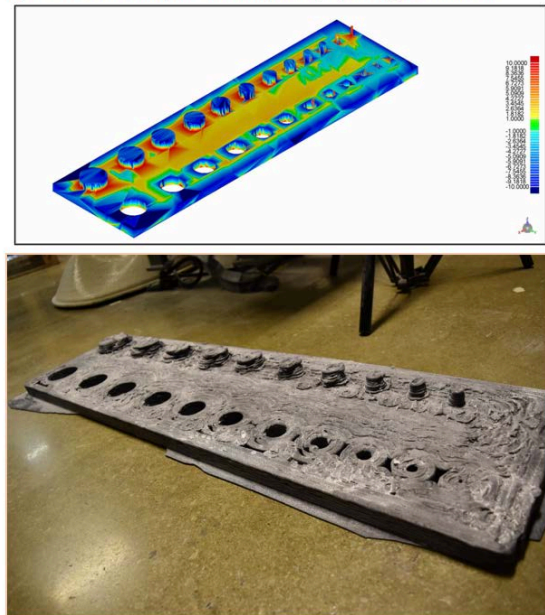


Figure 7: Deviation analysis on a scan of a sample print of pillars and holes.

Table 7: Deviation Distribution (Pillars and Holes)

>=Min	>Max	# Points	%	>=Min	>Max	# Points	%
-10.0000	-9.5909	631	0.1127	1.0000	1.4091	34313	6.1273
-9.5909	-9.1818	699	0.1248	1.4091	1.8182	26759	4.7784
-9.1818	-8.7727	817	0.1459	1.8182	2.2273	21547	3.8477
-8.7727	-8.3636	869	0.1552	2.2273	2.6364	20049	3.5802
-8.3636	-7.9545	901	0.1609	2.6364	3.0455	14772	2.6378
-7.9545	-7.5455	770	0.1375	3.0455	3.4545	10400	1.8571
-7.5455	-7.1364	733	0.1309	3.4545	3.8636	5204	0.9293
-7.1364	-6.7273	741	0.1323	3.8636	4.2727	1954	0.3489
-6.7273	-6.3182	1065	0.1902	4.2727	4.618	1486	0.2654
-6.3182	-5.9091	2464	0.4400	4.618	5.0909	1037	0.1852
-5.9091	-5.5000	3693	0.6595	5.0909	5.5000	1139	0.2034
-5.5000	-5.0909	4861	0.8680	5.5000	5.9091	1116	0.1993
-5.0909	-4.6818	4960	0.8857	5.9091	6.3182	1146	0.2046
-4.6818	-4.2727	5321	0.9502	6.3182	6.7273	967	0.1727
-4.2727	-3.8636	5321	0.9502	6.7273	7.1364	805	0.1437
-3.8636	-3.4545	6058	1.0818	7.1364	7.5455	561	0.1002
-3.4545	-3.0455	6515	1.1634	7.5455	7.9545	458	0.0818
-3.0455	-2.6364	6995	1.2491	7.9545	8.3636	442	0.0789
-2.6364	-2.2273	7123	1.2720	8.3636	8.7727	559	0.0998
-2.2273	-1.8182	8317	1.4852	8.7727	9.1818	676	0.1207
-1.8182	-1.4091	15747	2.8120	9.1818	9.5909	845	0.1509
-1.4091	-1.0000	23732	4.2378	9.5909	10.0000	1042	0.1861
-1.0000	1.0000	244573	43.6736				



Discussion

By accumulating data tables of deviation analysis of sample geometries like triangles, curved paths, holes and pillars, accumulating training sets for various purposes is now possible. 3D prints are prone to error at areas of sharp curvature, and given an arbitrary print, the curvature of a given tool path can be approximated numerically. If the tool path of the printer head is denoted $f(t) = (x(t), y(t))$, as in [6,9], then the curvature $\kappa(t) = \frac{|x'(t)y''(t) - y'(t)x''(t)|}{(x'^2 + y'^2)^{3/2}}$. Numerically, we

get

$$\kappa(t) \approx \left| \frac{x(t + \Delta t)y(t - \Delta t) + x(t)y(t + \Delta t) - y(t)x(t + \Delta t) - y(t + \Delta t)x(t - \Delta t) - x(t)y(t - \Delta t) + y(t)x(t + \Delta t)}{(\Delta t)^3} \right|$$

$$\left(\frac{(\Delta t)^2}{(x(t + \Delta t)^2 + y(t + \Delta t)^2 - 2x(t)x(t + \Delta t) - 2y(t)y(t + \Delta t) + x(t)^2 + y(t)^2)} \right)^{\frac{3}{2}} \text{ Error! No sequence specified,}$$

where $x(t)$ is the x-coordinate of the printer head in a layer, $y(t)$ is the y-coordinate, t is the time in the print, and Δt is the time step.

Subsets of a part's geometry can be partitioned to better understand what design parameters are feasible in the AM process. Since acute angles are a frequent cause of print error, the angle width in a layer of a part can be identified within a scan and added to the database that currently includes a few triangles. Error likelihood can be estimated as the training set grows. Similar understandings can be developed for areas with large numerical curvature and the shapes seen in tables 6 and 7. Correlation can be calculated between subset geometry size and curvature.

Similarly, analysis can be achieved through an online feedback mechanism. By attaching an IR camera to large-scale 3D printer extruders, deviation analysis can be conducted locally on the interior of part geometries. Statistical correlation can be calculated between numerous parameters of AM, including gantry velocity, flow rate, and tool path curvature. Infill tool path geometry can be classified in much the same way that the surface analysis can be studied using offline scans.

Training sets of these parameters, in both the online and offline setting, can lead to fairly basic but extremely helpful tools for designers and software developers. The mean deviation associated with various levels of curvature of a part can be easily computed. Computing the eigenvalues and eigenvectors of the correlation matrix of the surface deviations of various curvatures and knowing consistently successful geometries can help predict the likelihood of success of a print, as large eigenvalues indicate large variance from successful prints. Further data analysis and machine learning technologies can be applied to calculate how geometric variety affects the success of a print.

Similarly, in the online case, the likelihood of the success of a particular tool path can be classified by local curvature. If a particular segment of tool path exists frequently in poor-quality prints, as determined by the offline scan data, then design software can flag a user that a part geometry is not amenable to a print's success. If certain curvature values can be associated with successful prints, then a classification of tool paths can be constructed, whereby tool path optimization can be achieved. If outlier curvature values in a typically successful tool path frequently leads to print failure, then software can potentially automate the rejection of designs or tool paths containing those trajectories. These are all examples of potential strategies for utilization of the data acquired via the training sets developed.

The data from our tables show where particular part error occurs. As expected, sharp turns result in large protrusions around acute angles. For some prints, we get very narrow distributions, with most deviations extant around only a few standard deviations within each table. For instance, for the 80-10 triangles, 55.64% of the points were within 0-.1 cm from the CAD model; for the 50-

40 print, 38.39% of the points were within 0.0044 and 0.1036 cm of the CAD model. For other prints, we get more spread out distributions. Greater sample sets would be needed to determine a trend.

An analysis of the data begins to demonstrate when part failures and defections are more likely. At highly acute angles, we can see part defects and missing data from the original CAD model. We can also see more frequent and severe gap regions extending in triangles with greater acute angles. This occurs because, on the scale at which BAAM takes place, higher acceleration causes greater variance in bead width, propagating part defects throughout a print. This can also be seen in the pillars and holes build, in which defects can be found around the pillars and holes. In this print in particular, we learn that there is a limit on “pillar” size in a print. For the three smallest pillars in the print, the build experiences underfill problems, whereas the other pillars resulted in overfills. We also see missing data in the highest curvature regions of the sinusoidal prints.

Conclusion

In large scale AM systems, large data sets are needed to better understand the technology. By accumulating training sets on print quality, analysis can be done to correlate particular design parameters, tool paths, and printer settings with a successful build. The acquisition of such data can ultimately be used to program smarter robotic systems for better AM technologies.

To achieve these ends, two ways to acquire geometric deviation analysis on ORNL’s BAAM systems were outlined. A series of sample shapes were printed and laser scanned. Using the point clouds acquired from the laser scan, the difference between the cloud data and the surface of a CAD design was tested. This gave an online database which can now be drawn on for various purposes in software design. An online feedback system using an IR camera was also set up on the BAAM system. By collecting a video stream of the print, a deviation analysis can be similarly conducted and a training set built up, this time at each instance of the print.

With methods of developing training sets in hand, quality testing on every single printed object of the BAAM system can begin. These training sets can also be utilized in machine learning algorithm development. In this way, BAAM machines can be “taught” when prints will be successful, to what degree, and how they should react to improve print quality and success likelihood.

Acknowledgment of Funding

This material is based upon work supported by the U.S. Department of Energy, Office of Science, Office of [insert the sponsoring SC Program Office, e.g., Basic Energy Sciences], [*Add any additional acknowledgments or information requested by the sponsoring SC Program Office*] under contract number DE-AC05-00OR22725.

Notice of Copyright

This manuscript has been authored by UT-Battelle, LLC under Contract No. DE-AC05-00OR22725 with the U.S. Department of Energy. The United States Government retains and the publisher, by accepting the article for publication, acknowledges that the United States Government retains a non-exclusive, paid-up, irrevocable, worldwide license to publish or reproduce the published form of this manuscript, or allow others to do so, for United States Government purposes. The Department of Energy will provide public access to these results of federally sponsored research in accordance with the DOE Public Access Plan (<http://energy.gov/downloads/doe-public-access-plan>).

Works Cited

- [1] Tim Caffrey; Terry Wohlers. Wohlers Report 2015. Technical report, Wohlers Associates Inc., 2015.
- [2] R. Dinwiddle, M.M. Kirka, P. Lloyd, G.S. Marlow, " Calibrating IR cameras for in-situ temperature measurement during the electron beam melt process using Inconel 718 and Ti-Al6-V4." Conference: SPIE Commercial + Scientific Sensing and Imaging (June 2016).
- [3] Gibson I., Rosen D. W., et al., *Direct digital manufacturing* Additive manufacturing technologies, Springer, 2010; 363-384.
- [4] A. Hassen, R. Springfield, J. Lindahl, B. Post, L. Love, U. Viday, V. Kunc, and R.B. Pipes, "The Durability of Large-Scale Additive Manufacturing." Conference: CAMX (pending publication).
- [5] Q. Huang, H. Nouri, K. Xu, Y. Chen, S. Sosina and T. Dasgupta, "Predictive modeling of geometric deviations of 3D printed products - A unified modeling approach for cylindrical and polygon shapes," *2014 IEEE International Conference on Automation Science and Engineering (CASE)*, Taipei, 2014, pp. 25-30.
- [6] G.D. Knott. *Interpolating Cubic Splines*. Springer-Science-+Business Media, LLC, 2000.
- [7] Love L., Duty C., Post B., Lind R., Lloyd P., Kunc V., et al. Breaking Barriers in Polymer Additive Manufacturing. Oak Ridge National Laboratory (ORNL); Manufacturing Demonstration Facility (MDF); 2015.
- [8] L. Love, V. Kunc, O. Rios, C. Duty, A. Elliot, B. Post, R. Smith, and C. Blue, "The Importance of Carbon Fiber to Polymer Additive Manufacturing." *Journal of Materials Research*, 29(17), pp 1893-1898 (September 2014).
- [9] B.V. Ramana. *Higher Engineering Mathematics*. Tata McGraw-Hill Publishing Company Limited, 2006. New Delhi.
- [10] Reeves, Philip E. (1998) Reducing the surface deviation of stereolithography components. PhD thesis, University of Nottingham.

[11] Reeves, P.E. and Cobb, R.C., “*Surface deviation modelling of LMT processes - a comparative analysis*”, *5th European Conference on Rapid Prototyping & Manufacturing*, Dipoli Conference Centre, Helsinki, Finland, 5-7 June 1996.

[12] Xu, L., Huang, Q., Sabbaghi, A., and Dasgupta, T., 2013, “Shape Deviation Modeling for Dimensional Quality Control in Additive Manufacturing,” ASME Paper No. IMECE2013-66329.